# Structure and Function of the C-Terminal Domain of Methionyl-tRNA Synthetase†

Thibaut Crepin, Emmanuelle Schmitt, Sylvain Blanquet, and Yves Mechulam*

*Laboratoire de Biochimie, Unité Mixte de Recherche 7654, CNRS-Ecole Polytechnique, F-91128 Palaiseau Cedex, France*

*Received June 24, 2002; Revised Manuscript Received August 30, 2002*

ABSTRACT: The minimal polypeptide supporting full methionyl-tRNA synthetase (MetRS) activity is composed of four domains: a catalytic Rossmann fold, a connective peptide, a KMSKS domain, and a C-terminal α helix bundle domain. The minimal MetRS behaves as a monomer. In several species, MetRS is a homodimer because of a C-terminal domain appended to the core polypeptide. Upon truncation of this C-terminal domain, subunits dissociate irreversibly. Here, the C-terminal domain of dimeric MetRS from *Pyrococcus abyssi* was isolated and studied. It displays nonspecific tRNA-binding properties and has a crystalline structure closely resembling that of Trbp111, a dimeric tRNA-binding protein found in many bacteria and archaea. The obtained 3D model was used to direct mutations against dimerization of *Escherichia coli* MetRS. Comparison of the resulting mutants to native and C-truncated MetRS shows that the presence of the appended C-domain improves $tRNA^{Met}$ binding affinity. However, dimer formation is required to evidence the gain in affinity.

Methionyl-tRNA synthetase (MetRS) is a ubiquitous enzyme responsible for the specific aminoacylation of methionine transfer RNAs. Depending on the species from which it is isolated, MetRS behaves either as a monomer or a dimer. The reason for these two molecular states for a same enzyme activity is intriguing. Indeed, it was early demonstrated that dimeric *Escherichia coli* MetRS could be converted by C-terminal truncation into a minimal core of nearly 550 residues keeping activity for both the activation of methionine and the aminoacylation of $tRNA^{Met}$ (*1*). The truncated polypeptide can no more dimerize. Such shortened units derived from *E. coli* and *Thermus thermophilus* MetRS have been extensively studied, and in particular, the 3D structures of both enzymes were determined (*2*, *3*). The enzyme is made of four domains: a catalytic Rossmann fold, a connective peptide inserted between the two halves of the Rossmann fold, a KMSKS domain characteristic of class 1 aaRS (*4*−*6*), and a C-terminal α helix bundle domain, responsible for the recognition of the CAU anticodon of methionine tRNAs. These four domains form the structural core of MetRS and are systematically encountered in all MetRS sequenced so far (Figure 1). Thirty-four percent of known MetRS consist solely of this main unit and behave as monomers. The other MetRS (66%) contain domains appended to this minimal core and either form homodimers (48%) or remain long monomers (18%; Figure 1).

Dimer formation of MetRS is always related to the presence, at the C-side of the core enzyme, of an appended domain. Interestingly, some organisms express paralogs of this dimerization domain (Figure 1). Such paralogs are, for example, Trbp111[1] (tRNA-binding protein) of *Aquifex aeolicus* (*7*), the cold-shock protein CsaA from *B. subtilis* (*8*), yeast Arc1p (aminoacyl-tRNA cofactor protein, *9*), and the mammalian cytokine endothelial monocyte activating poly-

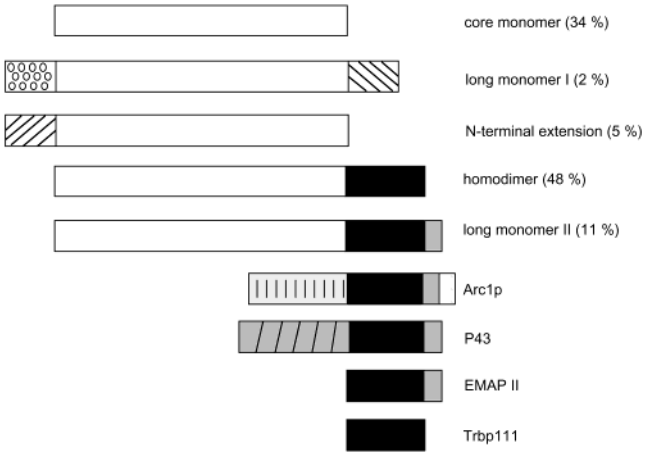


FIGURE 1: Structural organization of MetRS proteins and alignment of their C-terminal extensions with paralogous proteins. The open boxes represent the core structural unit of MetRS, whereas the dark boxes correspond to the C-terminal dimerization domain of MetRS. The light gray box schematizes the added domain in Arc1p, p43, EMAP II, and long monomer 1, which prevents dimerization. Other unrelated domains have specific patterns. The numbers in parentheses indicate the percentage of related oligomeric states according to a sample of 65 examined MetRS sequences. Bacterial MetRS belong either to the core monomeric or to the homodimeric type. In archaea, euryarchaeotal enzymes are monomeric, whereas crenarchaeotal enzymes are homodimeric. In eukaryotes, fungal MetRS present an N-terminal extension, whereas in viridiplantae and metazoa, these enzymes are long monomers. The 3D structure of the core monomer of MetRS is known in the cases of *E. coli* (*2*) and *T. thermophilus* (*3*). The 3D structures of human EMAP II (*14*, *15*) and *A. aeolicus* Trbp111 (*12*) have also been determined.

† Coordinates have been deposited at the Protein Data Bank with accession number 1MKH.

* Corresponding author. Tel: +33 1 69334885. Fax: +33 1 69333013. E-mail: yves@botrytis.polytechnique.fr.

[1] Abbreviations: SDS−PAGE, sodium dodecyl sulfate polyacrylamide gel electrophoresis; PCR, polymerase chain reaction; EDTA, ethylenediamine tetraacetic acid; EMAP II, endothelial monocyte activating polypeptide II; Arc1p, aminoacyl-tRNA cofactor protein; Trbp, tRNA-binding protein.

10.1021/bi026343m CCC: $22.00 
Published on Web 10/05/2002

peptide II (EMAP II, *10*). Both Arc1p and EMAP II interfere with the function of aminoacyl-tRNA synthetases in a trans-acting manner. Arc1p binds the N-terminal extension of monomeric MetRS of yeast, thereby increasing the affinity of the synthetase for tRNA (*9*). In mammals, a high molecular weight complex assembles nine aaRS with non-synthetase components. Cleavage of p43, one of these nonsynthetase components, by an apoptotic protease produces EMAP II (*11*).

The 3D structures of *A. aeolicus* Trbp111 (*12*), of *T. thermophilus* CsaA (*13*), and of human EMAP II (*14*, *15*) were determined. In all cases, an OB-fold forms the core of the structure. However, Trbp111 dimerizes, while EMAP II is monomeric. The monomeric state of EMAP II can be explained by a C-terminal extension (Figure 1), which masks the dimerization region (*15*). Interestingly, an EMAP II-like structure is found at the C-termini of long monomeric II MetRS (Figure 1), thereby explaining that these proteins cannot dimerize.

Biochemical characterizations show general tRNA-binding properties for both Trbp111 and EMAP II (*7*, *16*). Specificity of the binding appears rather broad, with recognition of the L shape of tRNA. It has been suggested that Trbp111 has the activity of a tRNA chaperone. Upon gene fusion, this activity would have been incorporated in MetRS, as well as in some other aminoacyl-tRNA synthetases such as PheRS and human TyrRS (*7*).

Here, we studied the C-terminal domain of dimeric MetRS from the archaeon *Pyrococcus abyssi*. Its three-dimensional structure was determined. This structure was used to direct mutations against the dimerization of *E. coli* MetRS. Study of the mutants indicates that the appended C-terminal domain is a cis-acting element providing the enzyme with a better tRNA affinity. However, to gain the increase in tRNA affinity, subunits of the enzyme must associate.

## RESULTS AND DISCUSSION

*Production and Characterization of the Dimerization Domain of MetRS.* The *metS* gene encoding MetRS from the hyperthermophilic archaeon *Pyrococcus abyssi* was PCR-amplified and cloned between the *Nco*I and *Sac*II sites of pET15blpa. In the resulting construction, the region encoding the His tag is removed. When expressed in *E. coli*, this vector leads to the production of two thermostable proteins. The heaviest protein has a molecular weight of 84 KDa, corresponding to that of *P. abyssi* MetRS (722 residues), whereas the lightest one has an apparent molecular weight of 12 KDa and is preponderant (Figure 2). To characterize this polypeptide, N-terminal sequencing was performed after excision of the protein from the gel. The sequence MYVKFD was obtained. It corresponds to an internal sequence of *P. abyssi* MetRS, starting at residue 616. Examination of the *metS* gene in this region shows that the ATG codon at position 616 is preceded 14 bases upstream by a putative AGGAGG Shine-Dalgarno sequence (*17*) (Figure 2). The polypeptide predicted to be produced from this ATG codon has a molecular weight of 12.4 KDa, in good agreement with the one observed upon SDS−PAGE analysis. This strongly indicates that the observed protein is produced from the ATG codon internal to *metS* and recognized as translation start signal by the *E. coli* ribosome. The protein was therefore called MetRS−C12K. At this stage, the possibility that MetRS−C12K is expressed in *Pyrococcus abyssi* remains open. Indeed, it should be underlined that the Shine-Dalgarno-like sequence AGGAGG is also complementary to a sequence at the 3′ end of the *P. abyssi* 16S rRNA (*18*). It might therefore represent a translation start signal in this species (*19*). To undertake the characterization of MetRS−C12K, the protein was purified from overproducing cells. Mass spectrometry measurements were performed, and confirmed the identity between the purified protein (12 041.6 ± 2.8 Da) and the one predicted from the gene sequence (12 041.2 Da). Moreover, as shown by molecular sieving, MetRS−C12K (30 $\mu$M) behaves as a dimer in solution.

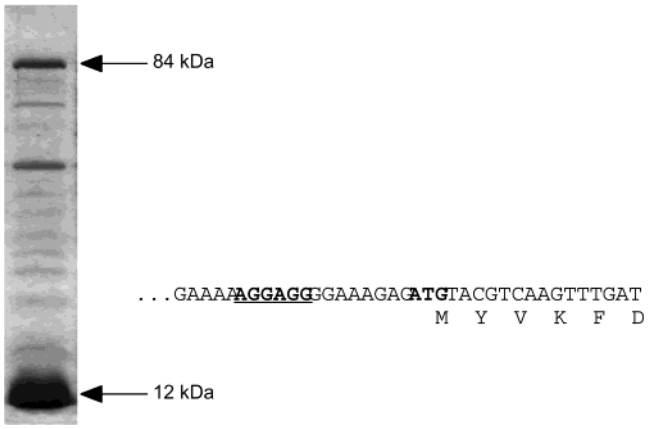


FIGURE 2: SDS−PAGE analysis of a heated extract of overproducing *E. coli* cells carrying the pET15bMet-pa plasmid. The bands corresponding to full-length *P. abyssi* MetRS (84 kDA) and to the isolated C-terminal domain (12 kDa) are flagged by arrows. The two other visible bands are also present in a nonoverproducing control extract and therefore correspond to thermostable *E. coli* proteins. In the left part of the figure, the sequence around the internal ATG codon corresponding to the start of MetRS−C12K is shown. The Shine−Dalgarno sequence is underlined.

As described in the Introduction section, MetRS−C12K belongs to a family of tRNA-binding proteins, including *A. aeolicus* Trbp111 (*7*), a part of the C-terminal domain of *S. cerevisiae* Arc1p (*9*), and the N-domain of the EMAP II cytokine (*10*, *16*). Trbp111 and Arc1p bind tRNAs with dissociation constants in the 10 nM range (*7*, *9*), whereas EMAP II binds tRNAs with an apparent $K_d$ of 20 $\mu$M (*16*). tRNA-binding properties of MetRS−C12K were studied by the gel-shift method. Assuming a stoichiometry of one tRNA molecule per dimer, experiments using purified *E. coli* $tRNA_f^{Met}$ or $tRNA_1^{Val}$ (0.5 $\mu$M) showed that MetRS−C12K can bind either of the two tRNAs with an equilibrium constant smaller than 0.5 $\mu$M (data not shown).

*Crystal Structure of MetRS*−C12K. Hexagonal crystals of MetRS−C12K were obtained by using 20% PEG8000 as precipitating agent in the presence of 50 mM potassium phosphate. Crystals belong to space group $P3_221$, with cell parameters $a = b = 38.3$ Å, $c = 161.6$ Å. Cryoprotection of the crystals could be achieved by soaking in a solution containing 10% ethylene glycol, 20% PEG8000, and 50 mM $KH_2PO_4$. A complete dataset to 2 Å of resolution was recorded at 100 K at the ESRF ID14-EH1 beamline. The structure was solved by molecular replacement by using residues 10−95 in the human EMAP II structure (*14*) as a starting model. The structure, containing one monomer per asymmetric unit, was refined to 2 Å resolution with *R* and

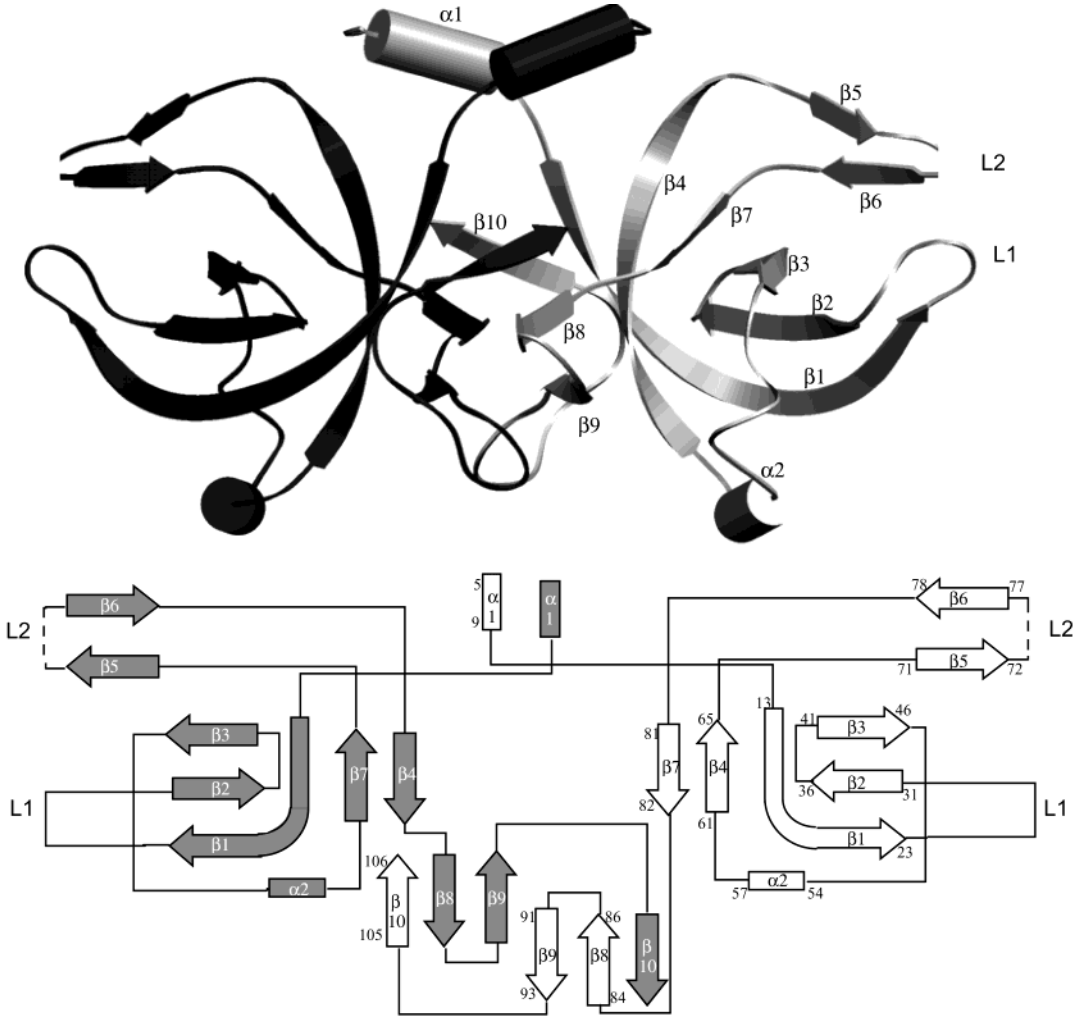


FIGURE 3: Structure of the dimeric MetRS−C12K domain. Top: representation of the 3D structure of the domain drawn with Setor (*46*). One monomer is colored in dark gray and the other monomer in light gray. Bottom: scheme of the topology showing secondary structure elements.

free-*R* values of 27.5% and 28.9%, respectively. The overall structure shows a *B* value of 69 Å$^2$, reflected at the level of the value of 49 Å$^2$ deduced from the Wilson plot of the diffraction data. This high *B* value is mainly due to two mobile loops (L1 and L2 in Figure 3), corresponding to residues 25−28 and 72−75, which have inaccurately determined positions (no density is observed for residue 74). Taking into account the small size of the protein, the presence of the two poorly ordered loops made it difficult to refine the structure to lower *R* values.

In the crystal, the structure of MetRS−C12K is homodimeric, with the dimer axis corresponding to a crystallographic axis. As shown in Figure 3, the structure of the subunit is mainly composed of $\beta$ strands. Only two short α helices are found, α1 at the N-terminus of the protein and α2 between $\beta$3 and $\beta$4. The structure defined by strands $\beta$1, $\beta$2, $\beta$3, $\beta$4, and $\beta$7 is reminiscent of that of an OB-fold (*20*), capped by the α2 helix. α1, $\beta$8, $\beta$9, and $\beta$10 ensure the dimer interface. Finally, it is remarkable that the interface of MetRS−C12K forms two symmetrical $\beta$ barrel-like structures (Figure 4). Therefore, on the whole, the MetRS−C12K dimer appears to result from the association of four $\beta$-barrels. The structure of MetRS−C12K is highly similar to those of Trbp111 from *A. aeolicus* (*12*) and CsaA from *T. thermophilus* (*13*). The rms deviation between MetRS−C12K and CsaA is 1.2 Å for 101 pairs of C α atoms. The model of the MetRS−C12K dimer can be superimposed on that of EMAP II (*14*, *15*) with an rmsd of 1.4 Å for 99 compared C alpha atoms. This superimposition involves C alpha atoms from both MetRS−C12K monomers, since the C-terminal extension of EMAP II aligns with the second monomer of MetRS−C12K. Such a superimposition reflects the previous observation that the C-terminal domain of monomeric EMAP II is related by degenerate 2-fold symmetry to the OB-fold domain, in such a way that the domain interface in EMAP II mimics the dimer interface of Trbp111-like proteins (*15*).

In the case of *A. aeolicus* Trbp111, binding of tRNA was studied by engineering site-directed mutants (*12*). The most important residues map in two loops. The first loop (L1) lies between $\beta$1 and $\beta$2, while the second loop (L2) connects $\beta$5 to $\beta$6. In MetRS−C12K, as in Trbp111, these two loops are face-to-face and form a clamp protruding out of the barrel (Figure 3). Most of the residues found important for tRNA binding in the case of Trbp111 are conserved in MetRS−C12K. These residues are K30 (L1), N66 and S78 (L2), and M81 (N-terminus of $\beta$7).

*Design of a Long Monomeric MetRS.* To investigate the role of the C-terminal domain in the context of MetRS, we wished to design mutations impairing the dimerization process. Our goal was to construct long monomers of *E. coli*

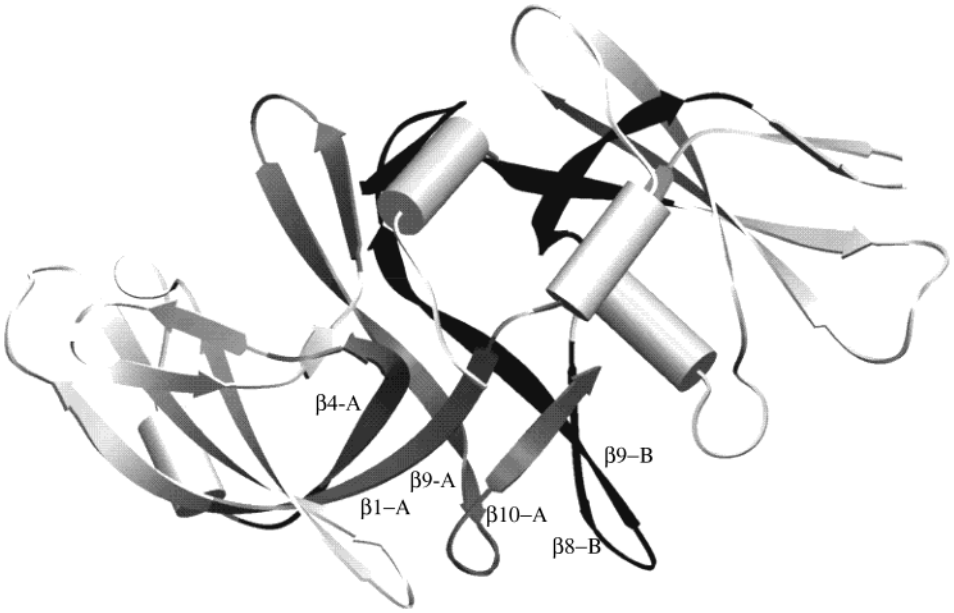


FIGURE 4: Dimer interface of MetRS−C12K. Top: schematic view of the MetRS−C12K dimer showing the internal $\beta$ barrel-like structure made upon dimerization. The secondary structure elements involved in the formation of this barrel are shown in dark gray for one monomer and in black for the other monomer. Only the bottom barrel is labeled; the symmetrical one is less visible, at the top of the view. For the sake of clarity, the $\beta$9−A and $\beta$9-B strands were prolonged by 4 residues at their C-termini.

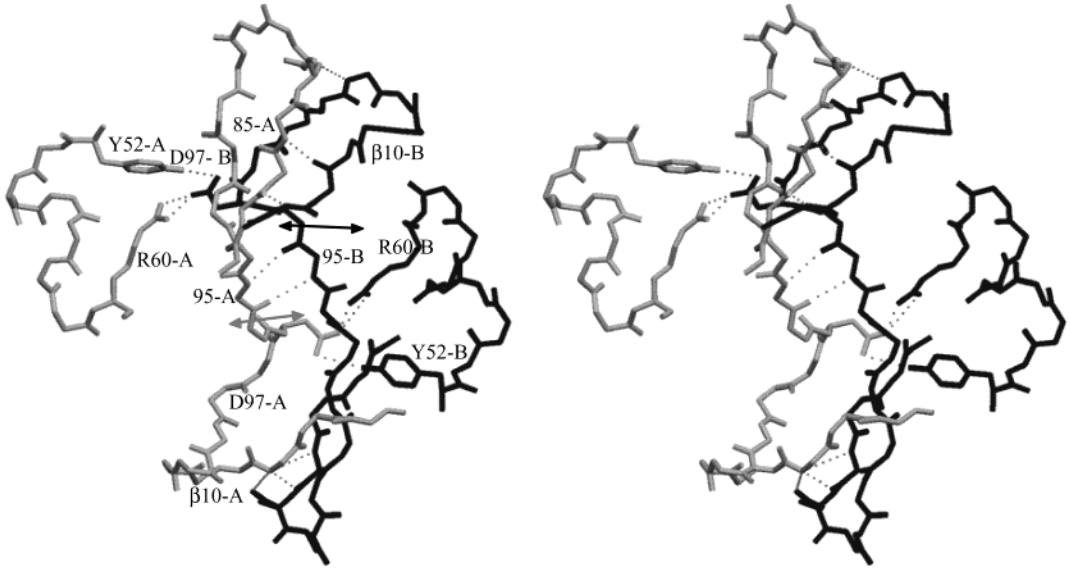


FIGURE 5: Stereo representation of the dimer interface modified by site-directed mutagenesis. The side chain interactions involving the conserved residues Tyr52 and Arg60 of one monomer and Asp96 of the other monomer are shown. The $\beta$ strands interactions between $\beta$10 and $\beta$8 are shown with dashed lines. The arrows indicate the position of the cleavage leading to the M665 variant. Only the relevant side chains are drawn.

MetRS to investigate the roles in enzyme activity of the C-terminal domain by itself on the one hand and of the dimerization of MetRS on the other hand. In MetRS−C12K, the dimer interface mainly results from antiparallel $\beta$-strand interactions. In addition, the two $\alpha$1 helices are packed together, and the N-termini are in contact through hydrogen bonds involving the carbonyl group of M1 of one monomer and the side chain of N67 of the other monomer. $\beta$ strand interactions involve the $\beta$10 C-terminal strand of one monomer, which contacts the $\beta$8 strand of the other monomer. In addition, the two symmetrical extended peptides after $\beta$9 (residues 95−97) also make main chain atom contacts (Figure 5). A notable exception is D97, whose side chain establishes electrostatic contacts with the side chains of Y52 and R60 of the other monomer (Figure 5). Y52 is strictly conserved in all dimeric Trbp111-like domains, while R60 and D97 only show conservative replacements at these positions (K or E, respectively). Interestingly, none of these residues is found in the monomeric EMAP II-like domains.

Because the dimer interaction primarily involves main chain atom contacts, mutations that cause dissociation of the dimer may be difficult to obtain. However, taking into account the interface contacts, we decided to construct two *E. coli* MetRS variants: the first one corresponds to the mutation into A of D666, the residue corresponding to D97 in MetRS−C12K (D666A mutant). In the second one, the $\beta$10 strand and the extended peptide at its N-terminus were removed by inserting a stop codon at position 666 (M665

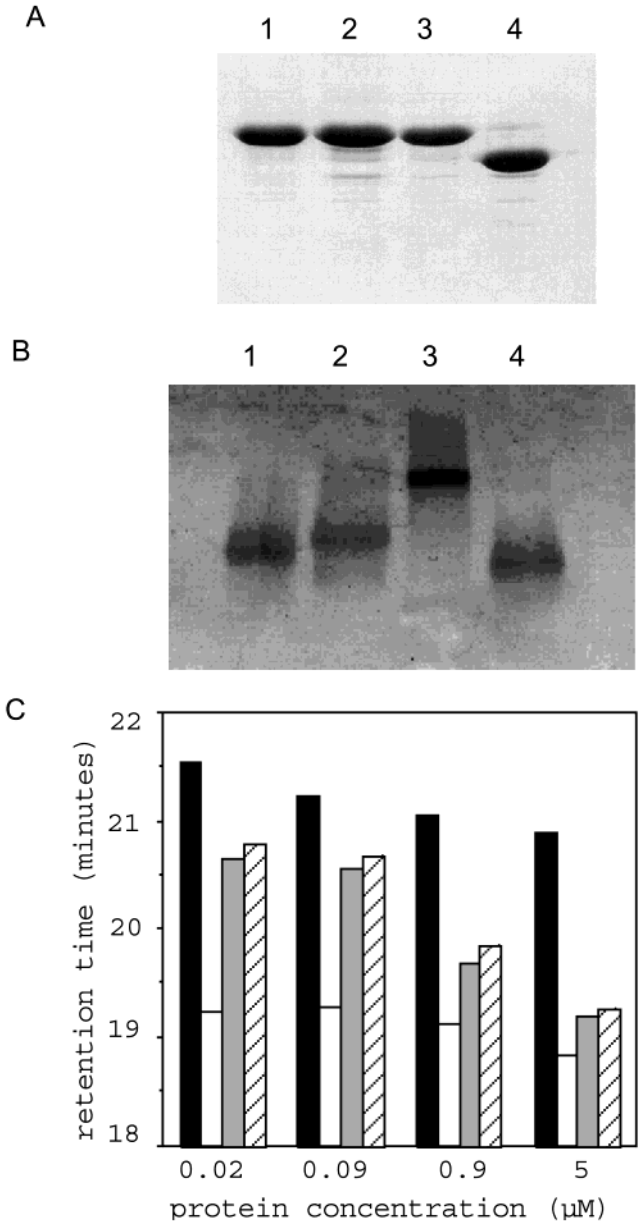


FIGURE 6: Panel A: SDS−PAGE analysis of MetRS variants. Lane 1, wild-type MetRS dimer; lane 2, M665; lane3, D666A; lane 4, M547 truncated monomer. Panel B: native PAGE analysis of MetRS variants. Electrophoresis of the purified proteins (6 $\mu$M) was performed on a 4−15% polyacrylamide gradient gel. Lane 1, M665; lane 2, D666A; lane 3, wild-type MetRS dimer; lane 4, M547 truncated monomer. Panel C: chromatographic analysis of MetRS variants. MetRS variants were injected at different concentrations onto a TSK4000SWXL molecular sieving column (TOSOHAAS 7.5 × 3000 mm) operated at 0.5 mL/min in 20 mM Tris. pH 7.6, 7 mM $MgCl_2$, 150 mM KCl. and 10 mM 2-mercaptoethanol. The retention times are indicated: filled bars M547, open bars M676, gray bars D666A, hatched bars M665. The indicated concentrations are those in the eluted peaks. Similar results were obtained in 20 mM Tris, pH 7.6, 10 mM $MgCl_2$.

mutant). The two variants could be overproduced as stable proteins in *E. coli* cells. They were purified to homogeneity, as judged by SDS−PAGE analysis (Figure 6). The thermal stabilities of the mutant enzymes were kept intact, as compared to that of the wild-type dimeric enzyme (half-life time of 16 min at 51 °C). The oligomeric states of D666A and M665 were studied by using native PAGE analysis and molecular sieving methods. As shown in Figure 6, the two mutant enzymes clearly behave as monomers on a native gel, although a faint band corresponding to the dimer is detectable in the case of D666A. Interestingly, when 10mM $MgCl_2$ is added to the gel buffer, the migration pattern of the D666A enzyme shifts toward that of the dimeric form, whereas M665 shows multiple bands indicative of an equilibrium between the monomeric and the dimeric forms (Figure 7C). Taking into account this salt-dependence, it appeared necessary to define the oligomeric state of the two mutants under the conditions routinely used for the biochemical characterization of MetRS. To achieve this, the retentions of the wild-type and mutant proteins on a HPLC molecular sieving column were compared (Figure 6). Two conditions were chosen: the first one corresponds to that used in the tRNA aminoacylation assay, i.e., 150 mM KCl plus 7 mM $MgCl_2$ (*21*), and the second one is that used in the fluorescence-monitored tRNA-binding assay (10 mM $MgCl_2$) (*22*). The results showed that, in either buffer, the mutants are monomeric, provided that their concentration is kept lower than 0.1 $\mu$M. Therefore, the two mutants must be monomeric under the conditions of the aminoacylation assay, where the catalyst is added at a concentration on the order of 0.3 nM. Although accurate dimer dissociation constants cannot be deduced from the chromatographic data, they could be estimated on the order of 1 $\mu$M for the two mutant proteins. As noted above, using PAGE analysis, the truncated M655 mutant appeared less prone to dimerization than the point mutant D666A. The whole data indicate that a mixture of monomers and dimers should form under the conditions of the tRNA-binding assay, when the enzyme concentration is in the micromolar range.

*Biochemical Characterization of the Mutant Enzymes.* The kinetic parameters of the two mutants were measured and compared to those of the dimeric M676 and minimal monomeric M547 enzymes (Table 2). Regarding the aminoacylation reaction, both mutant enzymes, monomeric in the assay, showed an increase in the Km of $tRNA_f^{Met}$. However, as compared to that with wild-type M676, the increase did not exceed a factor of 2. To facilitate comparisons, the $k_{cat}$ constants in Table 2 were systematically calculated for one protomer. Their values are slightly increased in the cases of one protomer of D666A or of one protomer of M665, as compared to one protomer of M676. The gains in $k_{cat}$ at saturating tRNA remain small, yet significant. Surprisingly, for the two mutants, the rate of the ATP−PPi exchange reaction was reduced by a factor of 2, whereas the $k_{cat}$ values are identical for M676 and M547 (*1* and Table 1). This might indicate that, in the presence of the C-terminal domain, dimerization influences the conformation of the active site. This effect is not reversed upon saturation of the tRNA-binding site, since the ATP−PPi exchange rates were not significantly changed in the presence of 5 $\mu$M $tRNA_f^{Met}$ (data not shown).

In a second set of experiments, the role of the C-terminal domain in tRNA binding was studied. Saturation of MetRS by $tRNA_f^{Met}$ causes an important quenching of the intrinsic enzyme fluorescence (*23*). This quenching is by 60% in the case of the M547 monomer and by 37% in the case of the M676 dimer. This difference can be explained by the anticooperative binding of a single tRNA molecule per dimer under the used conditions. Moreover, the dissociation constant of $tRNA_f^{Met}$ from the strong site in the M676 dimer

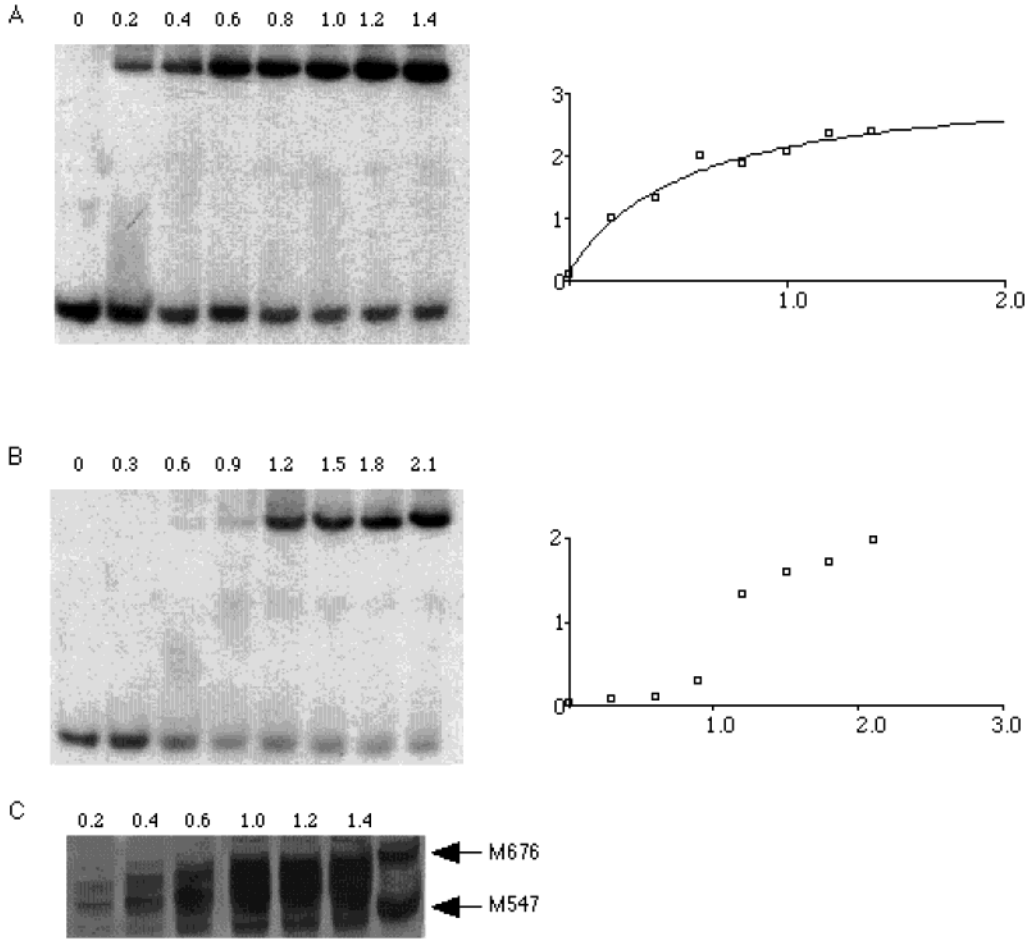


FIGURE 7: Binding of $tRNA_f^{Met}$ to MetRS variants. Panel A: gel shift assay of M676 associated to radioactively labeled $tRNA_f^{Met}$. The enzyme was incubated at increasing concentrations (0.2−1.4 $\mu$M) with 15 nM 5′-$^{32}$P-$tRNA_f^{Met}$ and electrophoresed on a native acrylamide gel. The curve on the right corresponds to a plot of the intensity of the shifted band as a function of enzyme concentration. It is fitted according to a simple binding equilibrium. Panel B: same experiment as that in panel A, with the M665 mutant. Panel C: same experiment as that in panel B, with the M665 mutant, but silver stained. This staining allows visualization of the proteins and shows the equilibrium between the monomeric and dimeric forms of M665 under the exact conditions of the gel shift assay. Migrations of M676 and M547 are indicated by arrows.

Table 1: Native Data Used in Structure Determination of MetRS−C12K[a]

| data set | native |
|---|---|
| X-ray source | ID14eh1 |
| unique reflections | 9286 |
| resolution (Å) | 2 |
| completeness | 97.3 (75.9) |
| redundancy | 3.0 (1.9) |
| $R_{sym}$ ($I$) (%)[b] | 5.2 (20.8) |
| $R$/free-$R$ (%) | 27.5/28.9 |
| rms deviatiations bonds (Å) | 0.0086 |
| angles (deg) | 1.53 |
| mean $B$ values (Å$^2$) protein atoms | 68.6 |
| water | 59.5 |

[a] Each data set was collected at 100 K with a single crystal. The values in parentheses correspond to the highest shell of resolution (2.06−2.01 Å). Note that the relatively low completeness is due to the 2.02−2.01 Å shell; completeness is 92.1% in the 2.07−2.02 Å shell. [b] $R_{sym}$ ($I$) = $[\sum_{hkl}\sum_i|\langle I_{hkl}\rangle - I_{hkl,i}|]/[\sum_{hkl}\sum_i|I_{hkl}|]$, where $i$ is the number of reflection $hkl$.

Table 2: Michaelis−Menten Parameters of the Aminoacylation Reaction and of the [32P]PPi-ATP Isotopic Exchange Catalyzed by Ec-MetRS Variants[a]

| | aminoacylation of $tRNA_f^{Met}$ | | [32P]PPi-ATP isotopic exchange | | tRNA binding |
|---|---|---|---|---|---|
| | $K_m$ ($\mu$M) | $k_{cat}$ ($s^{-1}$) | $K_m$ ($\mu$M) | $k_{cat}$ ($s^{-1}$) | $K_d$ ($\mu$M) |
| M676 | 4.4 ± 0.5 | 2.8 | 20 ± 3 | 42 | 0.20 ± 0.05 |
| M547 | 5.8 ± 0.7 | 3.6 | 22 ± 3 | 47 | 2.4 ± 0.4 |
| D666A | 6.4 ± 0.7 | 3.1 | 29 ± 4 | 23 | 0.40 ± 0.05 |
| M665 | 8.7 ± 1.0 | 4.4 | 34 ± 4 | 28 | 0.80 ± 0.2 |

[a] The values were determined by using homogeneous enzyme in standard assays as described in Materials and Methods. Parameters and standard errors were derived from iterative nonlinear least-squares fits of the Michaelis−Menten equation to the measured values. $k_{cat}$ values were calculated for one enzyme protomer. In the case of ATP−PPi isotopic exchange, $K_m$ is that of methionine measured at 2 mM ATP−$Mg^{2+}$. $K_d$ values were measured by spectrofluorometric titrations of the enzyme, assuming one tRNA-binding site per M547 monomer and one tRNA-binding site per dimer in the other cases.

(0.2 $\mu$M) is 12-fold lower than that from the single binding site on the M547 truncated monomer ($K_d$ value of 2.4 $\mu$M; *23* and Table 2). Affinity co-electrophoresis experiments showed a similar enhancement of the affinity of a $tRNA_f^{Met}$ acceptor microhelix to the M676 as compared to that of the M547 MetRS (*24*). In the cases of the M665 and D666A mutants, the quenchings upon tRNA saturation were by 40% and 37%, respectively. Such amplitudes rather argue in favor of a half of the site-binding behavior of the mutants in the titration assay. Nevertheless, dissociation constants of the two mutant enzyme:tRNA complexes were increased as

compared to that with the wild-type dimer (Table 2), showing that perturbation of the dimer interface had affected the strength of the tRNA binding.

Finally, formations of the enzyme:tRNA complexes were also studied by using a gel-shift assay for M676 and for the most affected mutant M665. In these experiments enzyme concentrations were varied in the range 0.2−2 $\mu$M. For the M676:tRNA complex, a $K_d$ value of 0.6 ± 0.2 $\mu$M could be deduced (Figure 7). This value agrees well with that obtained using affinity co-electrophoresis (*24*). With the M665 variant, the tRNA-binding curve displayed a sigmoidal shape, with a sharp transition at an enzyme concentration of 1.2 $\mu$M. This may indicate that tRNA preferentially binds the dimeric form of the enzyme. The oligomeric state of the mutant enzyme in the gel shift assay was assessed by silver staining of the proteins. As can be observed in panel C of Figure 7, the migration profile shows a multiple band pattern indicative of an equilibrium between the monomeric and the dimeric forms. Upon increasing the enzyme concentration, the amount of the dimeric form increases. Since the autoradiography shows a single shifted band, one can conclude that the enzyme:tRNA complex preferentially forms with the dimeric protein. The sharp transition of the curve could therefore be explained by similar equilibrium constants for dimer formation from M665 protomers and for tRNA binding by dimers of this mutant.

## CONCLUDING REMARKS

The data presented in this work establish that the C-terminal domain appended to dimeric MetRS provides the enzyme with additional tRNA-binding affinity, through general tRNA-binding properties. Therefore, this domain is indeed a structural and functional homologue of the Trbp111 protein.

*E. coli* MetRS mutants still containing the OB-folded tRNA-binding domain but affected in their capacity to dimerize were designed. Study of these mutants strongly indicates that the enhancement of tRNA-binding affinity conferred by the C-terminal domain is only expressed when the enzyme is in the dimeric state. The requirement for a dimeric form of the generic Trbp module to obtain full tRNA-binding affinity agrees with the low tRNA-binding affinity exhibited by monomeric EMAP II protein ($K_d$ of 20 $\mu$M, *16*). Moreover, the requirement for a dimeric state is in keeping with the previous proposal that the tRNA-binding cleft in Trbp111 is formed by both the L1-L2 loops and the dimer interface (*12*). In such a model, only one tRNA site can be occupied at a time, in agreement with the experimentally measured stoichiometry of one tRNA per Trbp111 dimer (*7*). This view also explains the anticooperative behavior observed for *E. coli* dimeric MetRS upon binding two tRNA molecules (*23*, *25*, *26*). Indeed, it was early demonstrated that the enzyme binds a first tRNA molecule with strong affinity, and a second one with a much lower affinity. It can be imagined that only the first bound tRNA benefits from an access to the C-terminal domain. In this context, the question whether the strongly bound tRNA cross bridges the MetRS subunits through other contacts remains open. Binding of the tRNA molecule might occur with the enzyme on one side and MetRS−C12K on the opposite side, as proposed by Nomanbhoy et al (*27*). The size of the linker peptide (20 residues) between the MetRS core and dimerization domain is sufficient to allow such a complex.

It has been previously proposed that the anticooperative binding of two tRNAs to dimeric MetRS might serve to couple the working conditions of the enzyme to the concentration of free $tRNA^{Met}$ (*25*). Indeed, at high tRNA concentration, occupation of the second weak binding site would stimulate tRNA dissociation from the strong binding site. However, under the conditions of the tRNA aminoacylation assay, the advantage in catalytic turnover of native MetRS as compared to the monomeric minimal core enzyme does not exceed a factor of 1.5 (*21*, Table 1). With the *Bacillus stearothermophilus* MetRS, the kinetic consequences of the anticooperative behavior are more apparent, with the occurrence of two sets of $K_m$ and $V_m$ values upon varying the tRNA substrate (*28*).

The case of *S. cerevisiae* MetRS is particular, since this monomeric enzyme associates with the Arc1p protein. This association confers on MetRS a much higher affinity for tRNA. However, it is notable that Arc1p, which contains an EMAP II-like C-terminal domain (Figure 1), is monomeric. In addition to this domain, Arc1p possesses an N-terminal domain important for MetRS binding and a central domain also involved in tRNA binding (*29*). It can be imagined that the central domain compensates for the absence of dimerization of this tRNA-binding protein.

Actually, nonessential appended tRNA-binding domains are also found in other aminoacyl-tRNA synthetases, such as yeast AspRS (*30*) or mammalian LysRS (*31*−*33*). In most cases, the catalytic parameters of the tRNA aminoacylation reaction are only slightly modified upon removal of these appended domains (see the cases of plant or human MetRS, *34* and *35*, or of mammalian LysRS, *31*−*33*). In contrast, the N-terminal appended domain of yeast AspRS and the interaction of yeast MetRS with Arc1p are associated to larger decreases of $K_m$ values for tRNA (*9*, *30*). Therefore, the understanding of the biological roles of these supplementary domains deserves further in vivo functional studies, as well as structural characterization of the complexes with tRNA. One idea is that these domains can be also involved in autoregulation of the expression of the aaRS genes. Such a genetic control has recently been evidenced in the case of yeast aspartyl-tRNA synthetase (M. Frugier and R. Giegé, Asilomar Conference on Aminoacyl-tRNA Synthetases, Pacific grove, CA, January 13−18, 2002). In the case of MetRS, regulation of the expression of the corresponding gene might benefit from the anticooperative behavior of the dimeric form. Indeed, it was earlier proposed that MetRS might down regulate the transcription of its own gene by binding a tRNA-like structure at the 5′ end of its mRNA (*36*). A dimeric structure of MetRS might be important in such a mechanism. Indeed, upon conditions of limiting free tRNA where the weak tRNA site remains unoccupied, the MetRS would strongly bind its mRNA. In contrast, in the presence of an excess of free tRNA, dissociation of the repressor MetRS from mRNA would be facilitated. Eventually, such a behavior would couple repressor binding and MetRS expression to the degree of aminoacylation of $tRNA^{Met}$.

## MATERIALS AND METHODS

*Expression and Purification of MetRS Variants.* In the case of *Pyrococcus abyssi*, the *metS* gene was PCR-amplified and cloned between the *Nco*I and *Sac*II sites of pET15lpa, a modified version of pET15b (Novagen). For the purification of MetRS−C12K, the resulting pET15bMet-pa was transformed into *E. coli* BL21-De3 cells. Cells were grown at 37 °C, in 1 L of 2xTY medium containing 50 $\mu$g/mL of ampicillin to an $OD_{650}$ of 1. After induction with 1 mM IPTG, cells were further grown during 15 h at 37 °C. Cells were harvested and resuspended in 30 mL of buffer A (10 mM MOPS pH6.7, 10 mM 2-mercaptoethanol, 0.1 mM PMSF) and disrupted by ultrasonic disintegration. The crude extract was centrifuged and the supernatant heated for 20 min at 80 °C. After centrifugation, the supernatant was loaded onto a Q-HiLoad ion exchange column (1.6 × 10 cm; Amersham) equilibrated in buffer A containing 50 mM NaCl. The protein was eluted stepwise with 1 M NaCl. The collected fractions were dialyzed against buffer A containing 50 mM NaCl. The protein was then loaded on an S-Sepharose high-performance column (1.1 × 4 cm; Amersham) equilibrated in the same buffer. Protein was eluted stepwise with 500 mM NaCl. The collected fractions (6 mL) were then directly loaded onto a Superdex 75 molecular sieving column (1.6 × 60 cm, Amersham) equilibrated in buffer A containing 500 mM NaCl. The resulting protein was finally dialyzed against buffer A containing 25 mM NaCl before storage at 4 °C. About 12 mg homogeneous protein was obtained.

Variants of the *E. coli* MetRS were produced by site-directed mutagenesis of the pBSM676 plasmid (*37*) using PCR techniques. Mutated MetRS were produced and purified as previously described (*38*).

*Mass Spectrometry and N-Terminal Sequencing.* A sample of MetRS−C12K protein (60 $\mu$M) was dialyzed against water and diluted to 6 $\mu$M in 50% acetonitrile containing 0.1% formic acid. Mass spectrometry experiments were performed on an electrospray spectrometer (Quattro II, Micromass, Manchester, U.K.).

For N-terminal sequencing, 12 $\mu$g of MetRS−C12K protein was loaded on a 12% SDS−polyacrylamide gel. After electrophoresis, the protein was electrotransferred onto a ProBlot membrane (Perkin-Elmer) and stained with amido black. The band containing the MetRS−C12K protein was cut and submitted to six cycles of automatic Edman degradation (Applied Biosystems 473A sequencer).

*Crystallization and Data Collection.* Initial screening for crystallization conditions of MetRS−C12K protein was performed at 4 °C with the hanging drop technique using protein at 6 mg/mL in storage buffer and commercial Crystal Screen solutions (Hampton Research). Hexagonal crystals were obtained using condition 42 of SM1 (20% PEG8000, 50 mM K−phosphate). The size of the crystals could be increased by using sitting drops at 24 °C. For data collection, the crystals were soaked during 1 min in 24% PEG8000, 50 mM $KH_2PO_4$ containing 10% ethyleneglycol as cryo-protectant, and flash cooled in liquid ethane. Data were collected at 100K using a synchrotronic source at the ESRF (ID14-EH1 beamline). Diffraction images were analyzed using Mosflm (A. G. W. Leslie, Laboratory of Molecular Biology, Cambridge, U.K.). Data were processed further with programs of the CCP4 package (*39*).

*Structure Determination and Refinement.* The structure was solved by molecular replacement by using human EMAP II (residues 10−95) as a starting model and the AMORE program (*40*). The structure was refined by cycles of manual model building using O (*41*) and conjugate gradient minimization using CNS (*42*). The final model contains 106 residues out of the 107 composing the MetRS−C12K protein and 16 water molecules. Residue R74 (loop L2) is disordered and has not been included in the model. In addition, the side chains of K4, K22, N26, D28, K29, K50, K53, E55, K72, and R90 were disordered, and the corresponding residues were therefore modeled as alanines. The final working and free *R*-factors were 27.5% and 28.9%, respectively, for the data to 2 Å resolution.

*Activity Measurements.* Methionine-dependent [$^{32}$P]PPi-ATP exchange activity was measured at 25°C in standard buffer (20 mM Tris-HCl, 7 mM $MgCl_2$, 10 mM 2-mercapto-ethanol, 0.1 mM EDTA, pH 7.6) containing 2 mM [$^{32}$P]PPi, 2 mM ATP and 2 mM methionine (*43*). Aminoacylation assays (*21*) were performed in the same standard buffer plus 150mM KCl, in the presence of 2 mM ATP, 50 $\mu$M L-[$^{14}$C]methionine (Amersham; 1.6 TBq/mol), and 5 $\mu$M *E. coli* $tRNA_f^{Met}$. For $K_m$ measurements, the concentration of tRNA was varied from 0.2 to 16 $\mu$M.

*Fluorescence at Equilibrium.* Variations of the intrinsic fluorescence of MetRS variants upon titration with $tRNA_f^{Met}$ were followed as described (*22*), at 25 °C, in 20 mM Tris-HCl (pH7.6), 10 mM 2-mercaptoethanol, 10 mM $MgCl_2$, and 0.1 mM EDTA. Saturation curves were obtained by varying the total concentration of $tRNA_f^{Met}$ (1250 pmol of methionine acceptance per $A_{260}$ unit, prepared from overproducing cells, *44*) from 0.03 to 3.6 $\mu$M. Dissociation constants were determined from iterative nonlinear least-squares fits of the theoretical equations to the experimental values, after correction for the inner filter effect (*22*). Confidence limits and standard errors were determined by 100 Monte Carlo simulations from the experimental deviations on individual measurements (*45*).

*Gel Shift Assay for tRNA Binding.* The gel shift assays were performed as described in ref *7*. *E. coli* MetRS variants were incubated at 4 °C at increasing concentrations with 15 nM 5′-[$^{32}$P]-labeled $tRNA_f^{Met}$ (1200 pmole/$A_{260}$ unit, purified as described in ref *44*), in a buffer containing 50 mM Tris−borate (pH 8.3), 5 mM $MgCl_2$, and 0.001% Triton X-100. The gel was run at 100 V for 3 h at 4 °C. After migration, the gel was dried onto a Nytran membrane and exposed on an X-ray film. Autoradiographies were then analyzed using the NIH-Image software. Silver staining was performed using the Bio-Rad kit, as recommended by the supplier.

## ACKNOWLEDGMENT

The authors are grateful to Sophie Bourcier (Laboratoire de Chimie des Mécanismes Réactionnels, Ecole Polytechnique) for determination of the Mw of MetRS−C12K by mass spectrometry and to Jacques d'Alayer and Maryline Davi (Laboratoire de Microséquençage des Protéines, Institut Pasteur, Paris) for protein sequencing. Thibaut Crépin was a recipient of a doctoral fellowship from the Association pour la Recherche sur le Cancer.

## REFERENCES


1. Cassio, D., and Waller, J. (1971) *Eur. J. Biochem. 20*, 283−300.
2. Mechulam, Y., Schmitt, E., Maveyraud, L., Zelwer, C., Nureki, O., Yokoyama, S., Konno, M., and Blanquet, S. (1999) *J. Mol. Biol. 294*, 1287−97.
3. Sugiura, I., Nureki, O., Ugaji-Yoshikawa, Y., Kuwabara, S., Shimada, A., Tateno, M., Lorber, B., Giege, R., Moras, D., Yokoyama, S., and Konno, M. (2000) *Struct. Fold. Des. 8*, 197−208.
4. Hountondji, C., Dessen, P., and Blanquet, S. (1986) *Biochimie 68*, 1071−1078.
5. Eriani, G., Delarue, M., Poch, O., Gangloff, J., and Moras, D. (1990) *Nature 347*, 203−206.
6. Cusack, S., Härtlein, M., and Leberman, R. (1991) *Nucleic Acids Res. 19*, 3489−3498.
7. Morales, A. J., Swairjo, M. A., and Schimmel, P. (1999) *EMBO J. 18*, 3475−83.
8. Muller, J. P., Bron, S., Venema, G., and van Dijl, J. M. (2000) *Microbiology 146*, 77−88.
9. Simos, G., Segref, A., Fasiolo, F., Hellmuth, K., Shevchenko, A., Mann, M., and Hurt, E. C. (1996) *EMBO J. 15*, 5437−48.
10. Kao, J., Ryan, J., Brett, G., Chen, J., Shen, H., Fan, Y. G., Godman, G., Familletti, P. C., Wang, F., Pan, Y. C., and et al. (1992) *J. Biol. Chem. 267*, 20239−47.
11. Shalak, V., Kaminska, M., Mitnacht-Kraus, R., Vandenabeele, P., Clauss, M., and Mirande, M. (2001) *J. Biol. Chem. 276*, 23769−76.
12. Swairjo, M. A., Morales, A. J., Wang, C. C., Ortiz, A. R., and Schimmel, P. (2000) *EMBO J. 19*, 6287−98.
13. Kawaguchi, S.-I., Müller, J., Linde, D., Kuramitsu, S., Shibata, T., Inoue, Y., Vassylyev, D., and Yokoyama, S. (2001) *EMBO J. 20*, 562−569.
14. Kim, Y., Shin, J., Li, R., Cheong, C., Kim, K., and Kim, S. (2000) *J. Biol. Chem. 275*, 27062−8.
15. Renault, L., Kerjan, P., Pasqualato, S., Menetrey, J., Robinson, J. C., Kawaguchi, S., Vassylyev, D. G., Yokoyama, S., Mirande, M., and Cherfils, J. (2001) *EMBO J. 20*, 570−8.
16. Quevillon, S., Agou, F., Robinson, J. C., and Mirande, M. (1997) *J. Biol. Chem. 272*, 32573−9.
17. Shine, J., and Dalgarno, L. (1974) *Proc. Natl. Acad. Sci. U.S.A. 71*, 1342−1346.
18. Lecompte, O., Ripp, R., Puzos-Barbe, V., Duprat, S., Heilig, R., Dietrich, J., Thierry, J. C., and Poch, O. (2001) *Genome Res. 11*, 981−93.
19. Tompa, M. (1999) *Proc. Int. Conf. Intell Syst. Mol. Biol*. 262−71.
20. Murzin, A. G. (1993) *EMBO J. 12*, 861−7.
21. Lawrence, F., Blanquet, S., Poiret, M., Robert-Gero, M., and Waller, J. P. (1973) *Eur. J. Biochem. 36*, 234−43.
22. Blanquet, S., Petrissant, G., and Waller, J. P. (1973) *Eur. J. Biochem. 36*, 227−33.
23. Blanquet, S., Iwatsubo, M., and Waller, J. P. (1973) *Eur. J. Biochem. 36*, 213−26.
24. Gale, A. J., Shi, J. P., and Schimmel, P. (1996) *Biochemistry 35*, 608−15.
25. Blanquet, S., and Dessen, P. (1976) *J. Mol. Biol. 103*, 765−84.
26. Dessen, P., Blanquet, S., Zaccai, G., and Jacrot, B. (1978) *J. Mol. Biol. 126*, 293−313.
27. Nomanbhoy, T., Morales, A. J., Abraham, A. T., Vortler, C. S., Giege, R., and Schimmel, P. (2001) *Nat. Struct. Biol. 8*, 344−8.
28. Kalogerakos, T., Dessen, P., Fayat, G., and Blanquet, S. (1980) *Biochemistry 19*, 3712−23.
29. Simos, G., Sauer, A., Fasiolo, F., and Hurt, E. C. (1998) *Mol. Cell 1*, 235−42.
30. Frugier, M., Moulinier, L., and Giege, R. (2000) *EMBO J. 19*, 2371−80.
31. Shiba, K., Stello, T., Motegi, H., Noda, T., Musier-Forsyth, K., and Schimmel, P. (1997) *J. Biol. Chem. 272*, 22809−16.
32. Stello, T., Hong, M., and Musier-Forsyth, K. (1999) *Nucleic Acids Res. 27*, 4823−9.
33. Francin, M., Kaminska, M., Kerjan, P., and Mirande, M. (2002) *J. Biol. Chem. 277*, 1762−9.
34. Kaminska, M., Deniziak, M., Kerjan, P., Barciszewski, J., and Mirande, M. (2000) *EMBO J. 19*, 6908−17.
35. Kaminska, M., Shalak, V., and Mirande, M. (2001) *Biochemistry 40*, 14309−14316.
36. Dardel, F., Panvert, M., and Fayat, G. (1990) *Mol. Gen. Genet. 223*, 121−33.
37. Mellot, P., Mechulam, Y., Le Corre, D., Blanquet, S., and Fayat, G. (1989) *J. Mol. Biol. 208*, 429−43.
38. Fourmy, D., Meinnel, T., Mechulam, Y., and Blanquet, S. (1993) *J. Mol. Biol. 231*, 1068−77.
39. Collaborative computational project No.4. (1994) *Acta Cristallogr. D50*, 760−763.
40. Navaza, J. (1994) *Acta Cryst A50*, 157−163.
41. Jones, T. A., Zou, J. Y., Cowan, S. W., and Kjeldgaard, M. (1991) *Acta Crystallogr. A47*, 110−119.
42. Brunger, A. T., Adams, P. D., Clore, G. M., DeLano, W. L., Gros, P., Grosse-Kunstleve, R. W., Jiang, J. S., Kuszewski, J., Nilges, M., Pannu, N. S., Read, R. J., Rice, L. M., Simonson, T., and Warren, G. L. (1998) *Acta Crystallogr. D54*, 905−21.
43. Blanquet, S., Fayat, G., Waller, J. P., and Iwatsubo, M. (1972) *Eur. J. Biochem. 24*, 461−9.
44. Meinnel, T., and Blanquet, S. (1995) *J. Biol. Chem. 270*, 15908−15914.
45. Dardel, F. (1994) *Comput. Applic. Biosci. 10*, 273−275.
46. Evans, S. V. (1993) *J. Mol. Graphics. 11*, 134−138.


BI026343M